Generative Design of Multi-Material Hierarchical Structures via Concurrent Topology Optimization and Conformal Geometry Method

Conference Paper · August 2019

DOI: 10.1115/DETC2019-97617

CITATION
1

READS
103

3 authors:

Long Jiang
Ford Motor Company
11 PUBLICATIONS **64** CITATIONS
SEE PROFILE

Shikui Chen
Stony Brook University
51 PUBLICATIONS **1,197** CITATIONS
SEE PROFILE

Xianfeng David Gu
Stony Brook University
412 PUBLICATIONS **7,789** CITATIONS
SEE PROFILE

Proceedings of the ASME 2019 International Design Engineering Technical Conferences & Computers and Information in Engineering Conference
IDETC/CIE 2019
August 18 – 21, 2019, Anaheim, CA, USA

DETC2019-97617

GENERATIVE DESIGN OF MULTI-MATERIAL HIERARCHICAL STRUCTURES VIA CONCURRENT TOPOLOGY OPTIMIZATION & CONFORMAL GEOMETRY METHOD

Long Jiang[1]
[1]Department of Mechanical Engineering
State University of New York
at Stony Brook
Stony Brook, NY 11794, USA
Email: long.jiang@stonybrook.edu

Shikui Chen[1,*]
[1]Department of Mechanical Engineering
State University of New York
at Stony Brook
Stony Brook, NY 11794, USA
Email: shikui.chen@stonybrook.edu

Xianfeng David Gu[2]
[2]Department of Computer Science
State University of New York
at Stony Brook
Stony Brook, NY 11794, USA
Email: gu@cs.stonybrook.edu

ABSTRACT

Topology optimization has been proved to be an automatic, efficient and powerful tool for structural designs. In recent years, the focus of structural topology optimization has evolved from mono-scale, single material structural designs to hierarchical multimaterial structural designs. In this research, the multi-material structural design is carried out in a concurrent parametric level set framework so that the structural topologies in the macroscale and the corresponding material properties in mesoscale can be optimized simultaneously. The constructed cardinal basis function (CBF) is utilized to parameterize the level set function. With CBF, the upper and lower bounds of the design variables can be identified explicitly, compared with the trial and error approach when the radial basis function (RBF) is used. In the macroscale, the 'color' level set is employed to model the multiple material phases, where different materials are represented using combined level set functions like mixing colors from primary colors. At the end of this optimization, the optimal material properties for different constructing materials will be identified. By using those optimal values as targets, a second structural topology optimization is carried out to determine the exact mesoscale metamaterial structural layout. In both the macroscale and the mesoscale structural topology optimization, an energy functional is utilized to regularize the level set function to be a distance-regularized level set function, where the level set function is maintained as a signed distance function along the design boundary and kept flat elsewhere. The signed distance slopes can ensure a steady and accurate material property interpolation from the level set model to the physical model. The flat surfaces can make it easier for the level set function to penetrate its zero level to create new holes. After obtaining both the macroscale structural layouts and the mesoscale metamaterial layouts, the hierarchical multimaterial structure is finalized via a local-shape-preserving conformal mapping to preserve the designed material properties. Unlike the conventional conformal mapping using the Ricci flow method where only four control points are utilized, in this research, a multi-control-point conformal mapping is utilized to be more flexible and adaptive in handling complex geometries. The conformally mapped multi-material hierarchical structure models can be directly used for additive manufacturing, concluding the entire process of designing, mapping, and manufacturing.

1 Introduction

With the rapid development of the structural design methodology and the modern additive manufacturing technology, in recent years, building multiscale structures with space-varying metamaterials has become possible [1, 2, 3]. On the other hand, by introducing different construction materials to be redistributed inside the design domain properly, the final multimaterial structure can be expected to have a performance boost [4]. Besides, introducing multiple constructing materials can make

*Address all correspondence to this author.

some design objectives easier to be achieved, compared with using only one material [5]. This paper is aiming at designing hierarchical multimaterial structures

Topology optimization is a powerful and advanced tool for designing structures with high performances. There are a number of different approaches in this field and a comparative review between can be found in [6]. Among those approaches, the level set methods stand out for its flexibility in handling topological changes and in generating clear design boundaries [7, 8, 9]. For more details about the level set methods, the readers can be referred to [10] for more information. Generally, by using the zero level of the level set function to model the structural design boundary [11], one level set function can separate the design domain into two sub-domains: the void domain and the material domain. However, when two or more material phases have to be included, this implicit boundary representation has to be modified accordingly. The 'color' level set method [12], the piecewise constant level set method [13] and the reconciled level set method [14] are several widely used schemes for modeling multiple material phases within the level set framework. In this paper, the 'color' level set method is utilized. Similar to mixing colors from three primary colors, the 'color' level set method uses n different level set functions to represent up to 2^n different material domains. Therefore, the overall effective material property can be interpolated by assembling the separate constitutive material together with the help of the Heaviside function of each level set function.

On the other hand, structures with multiple scales possess fine-tuned mesoscale filling properties with a low overall density [15, 16, 17]. Thus, they can be found in a wide range of engineering applications [18]. In multiscale or hierarchical structure designing, the key issue is to find the constructing metamaterials with tailored properties. Within the level set framework, the metamaterial designs have covered the topics of designing the negative permeability metamaterails [19], the negative Poisson's ratio metamaterials [20, 21], the electromagnetic metamaterials [22], the zero/negative thermal expansion metamaterials [23] and so on. However, only designing the metamaterial to be filled inside the macroscale structure can not fully explore the potential of the multiscale structure. Ideally, the mesoscale structures and the macroscale structures should be designed in a concurrent manner since the macroscopic loading and boundary conditions will affect not only the macroscale overall structural layout, but also the optimal mesoscale metamaterial properties. Sivapuram et al. [24] developed the concurrent structural topology optimization for multiscale structures where the mesoscale metamaterials have fixed pre-defined locations. Wang et al. [25] proposed the concurrent design of multiscale structures filled with spatially-varying graded microstructures to ensure the connectivity between adjacent mesoscale units. Both Sivapuram's work with pre-defined metamaterial locations and Wang's work with similar topological feature metamaterials are all meant to alleviate the heavy computational cost of introducing too many different types of metamaterials in different locations. Another approach for the concurrent design of multiscale structure is proposed by Li et al. [26], where the density based method is employed in the macroscale and the level set approach is employed in the mesoscale. The mesoscale metamaterial is determined by the intermediate density generated from the macroscale optimization. This combination converts the undesired intermediate densities of the density based approach into an advantage of the entire design methodology and the numerical examples have verified the effectiveness of this process.

Conventionally, the level set methods use a virtual velocity field derived from the sensitivity analysis to evolve the design boundary [27, 28, 7] and solve the Hamilton-Jacobi partial differential equation (PDE) to describe the dynamics of the boundary motion [29]. However, this level set framework faces some drawbacks [30, 31]. A promising solution is to employ the parameterized level set method [32]. Combined with mathematical programming and the gradient-based optimizer MMA [33], introducing multiple design constraints can become straightforward and the numerical efficiency can be improved. The optimal structure generated via parametric level set approach has also been reported having the advantage of requiring less prefabrication time for additive manufacturing [34], which is a preferred feature for combining designing with applications. However, when the radial basis function (RBF) is used in the conventional parametric level set method (PLSM) [30, 35], the upper and lower bounds for the design variable can not be explicitly identified. Therefore, in our previous research, a cardinal basis function (CBF) is proposed [36] to replace the RBF kernel function. With CBFs, the design variable bounds can be explicitly set to be the lower and upper bounds of the corresponding level set function, avoiding the trial and error approach when the RBF kernel function is used. Moreover, by introducing a distance regularization energy functional [37] to regularize the shape of the level set function throughout the optimization process, the level set function can be maintained a distance-regularized shape for an accurate material property interpolation. The flat surfaces of the distance-regularized level set function can stabilize the optimization process and can help to create of new holes [36].

This paper further develops our previous concurrent topology optimization of multiscale structures [38, 39] from single material to multiple materials. The 'color' level set method is utilized for the multimaterial representation. On the macroscale, the overall structural topology and the optimal corresponding mesoscale metamaterial properties are optimized simultaneously. By using the optimal metamaterial properties as targets, a second optimization process is carried out to find out the structural layout with an isotropy constraint [40, 41, 42]. The structural topology optimization on both scales are all carried out within the CBF-based parametric level set method framework. The distance regularization energy functional is minimized during the

optimization process to maintain the distance-regularized shape of the level set functions. After achieving the structural layouts for both scales, the angle-preserving conformal mapping is employed to finalize the multiscale structure. The angle-preserving mapping characteristic and the isotropy of the mesoscale metamaterials can mathematically ensure the consistency of the material properties after the mapping of the multiscale structure.

The remaining paper is organized as follows. In section 2, the 'color' level set method for designing multimaterial structure is introduced. The CBF kernel functions and the concurrent parametric level set function are detailed in section 3. Section 4 presents the mesoscale metamaterial design and the multi-control-point conformal mapping technique used for multiscale structure finalization.The numerical examples are listed in section 5. The conclusions are drawn in section 6.

2 'Color' Level Set Model for Multimaterial Representation

In the conventional level set representation with a single level set function, the design boundary is implicitly described as the zero level of the one dimensional higher level set function [8, 7]. However, when multiple structure phases are introduced, the number of the level set functions has to increase as well. With the 'color' level set representation, n level set functions can divide the design domain into up to 2^n different regions. The level set functions used can be described as:

$$\begin{cases} \Phi_k(\boldsymbol{x}) > 0, & (\boldsymbol{x} \in \Omega_k \setminus \Gamma_k) \\ \Phi_k(\boldsymbol{x}) = 0, & (\boldsymbol{x} \in \Gamma_k), \quad k = 1,...,n \\ \Phi_k(\boldsymbol{x}) < 0, & (\boldsymbol{x} \in D \setminus \Omega_k \cup \Gamma_k) \end{cases}. \tag{1}$$

In Eq. 1, Φ_k denotes the kth level set function and Ω_k, Γ_k represent the region where the kth level set function has positive value and its corresponding boundary, respectively. D represents the design domain. The example of identifying different regions inside the design domain by the sign of the level set function is illustrated in Figure 1.

With this 'color' level set representation, each material phase can be represented by combining different level set functions together. For example, the elastic tensor of a two-material structure at a given point $\boldsymbol{x}$ can be expressed as:

$$\boldsymbol{D}^{(2)}(\boldsymbol{x},\Phi) = H(\Phi_1)\{[1-H(\Phi_2)]\boldsymbol{D}_1 + H(\Phi_2)\boldsymbol{D}_2\} + [1-H(\Phi_1)]\boldsymbol{D}_0. \tag{2}$$

In Eq.2, the $D^{(2)}$ represents the interpolated elastic tensor with two materials. The $H(\Phi)$ is the Heaviside function of the level set function Φ. $\boldsymbol{D}_1$ and $\boldsymbol{D}_2$ are the elastic tensors of two different constructing materials.The $\boldsymbol{D}_0$ is a dummy elastic tensor with a small positive value to avoid singularities. Generally, as

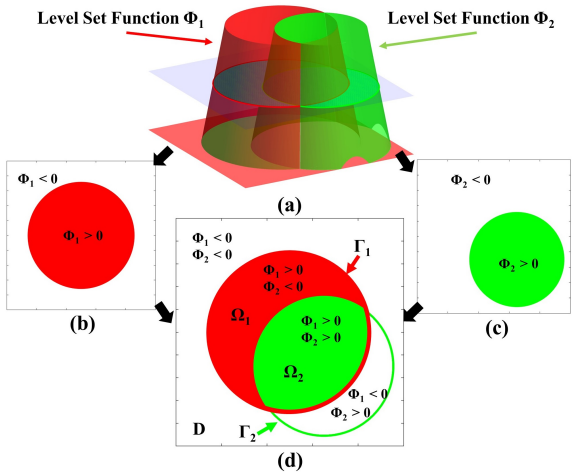

FIGURE 1. The 'color' level set representation. (a) The two level set functions. (b) The sign of level set function 1. (c) The sign of level set function 2. (d) The combination of two level set functions. In this research Ω_1 represents the 1st material phase with boundary Γ_1 and Ω_2 represents the 2nd material phase with boundary Γ_2. The reset regions are considered as void inside the design domain D.

can be seen from Figure 1, the level set function Φ_1 is used to distinguish the material region from the void region. Next, inside the material region, the level set function Φ_2 is used to determine whether the given region should have the material property 1 or 2. With this 'color' level set, the material property inside the design domain can be calculated. Although the whole process is similar to the multimaterial representation of the density-based approach, the 'color' level set scheme can retain the clear design boundary advantage of the level set methods.

3 Concurrent Macro-scale and Meso-scale Optimization with CBF-based Parametric Level Set Method (PLSM)

With a given kernel function at the jth node as Ψ_j, the kth level set functions for multimaterial representation can be parameterized into the following form:

$$\Phi_k(\boldsymbol{x}) = \sum_{j=1}^{m} \Psi_j(\boldsymbol{x})\mu_{kj}, \quad k = 1,...n. \tag{3}$$

In conventional parametric level set method, the kernel function is commonly selected as the RBF. However, with a given support radius, the neighbouring RBF kernel functions will overlap with each other. Therefore, the corresponding weights, namely μ_{kj} in Eq.3, do not have a clear upper and lower bounds. As the design variables [30], those bounds should be passed to

the optimizer explicitly. This issue can be solved by constructing the cardinal basis function (CBF) as the kernel function for the level set function parameterization [36]. The CBF has the Kronecker delta property as:

$$\Psi_j(x_i) = \begin{cases} 1, \ (if \ i = j) \\ 0, \ (if \ i \neq j) \end{cases} \ j = 1, ..., m. \tag{4}$$

When the CBF is used for the level set function parameterization, the corresponding weights will be the upper and lower bounds of the level set function itself. This explicit bounds can maintain the numerical stability of the optimizer and avoid the trial and error approach for guessing those bounds.

Generally, a multimaterial optimization for minimal mean structural compliance can be formulated as:

$$\begin{aligned} Min: \quad & J = \int_D \boldsymbol{\varepsilon}(\boldsymbol{u}) : \boldsymbol{D}^* : \boldsymbol{\varepsilon}(\boldsymbol{u}) d\Omega \\ s.t.: \quad & a \ (\boldsymbol{u}, \boldsymbol{v}, \Phi) = l(\boldsymbol{v}, \Phi) \\ & Vol_k \leq Vol_k^t, \quad (k = 1, ..., n) \\ & \mu_{kj}^L \leq \mu_{kj} \leq \mu_{kj}^U, \quad (j = 1, ..., m). \end{aligned} \tag{5}$$

In Eq.5, the $\boldsymbol{\varepsilon}(\boldsymbol{u}) : \boldsymbol{D}^* : \boldsymbol{\varepsilon}(\boldsymbol{u})$ represents the stain energy density of the structure with a elastic tensor $\boldsymbol{D}^*$ calculated from the aforementioned 'color' level set multimaterial representation. $\boldsymbol{u}$ is the displacement field and $\boldsymbol{v}$ is the test function. The kth material has the volume of Vol_k that is constrained by its volume target Vol_k^t. At most, the number of different material phases can reach to 2^n. However, in this paper, this is simplified to only n different phases. The lower and upper bounds for the design variable μ_{kj} can be easily get from the upper and lower bound of the corresponding level set function. The energy bilinear form $a(\boldsymbol{u}, \boldsymbol{v}, \Psi)$ and the load linear form $l(\boldsymbol{v}, \Psi)$ are detailed as:

$$\begin{aligned} a \ (\boldsymbol{u}, \boldsymbol{v}, \Phi) &= \int_D \boldsymbol{\varepsilon}(\boldsymbol{u}) : \boldsymbol{D}^* : \boldsymbol{\varepsilon}(\boldsymbol{u}) d\Omega \\ l \ (\boldsymbol{v}, \Phi) &= \int_\Gamma \boldsymbol{t} \cdot \boldsymbol{v} d\Gamma. \end{aligned} \tag{6}$$

To calculate the volume for each material phase, the following equation can be formulated:

$$Vol_k = \int_D \prod_{i=1}^{k} H(\Phi_i) d\Omega, \quad i = 1, ..., n. \tag{7}$$

This volume fraction formulation can be understood in a more intuitive way. For example, when 2 level set functions are used, the total number of potential material phases can reach up to $2^2 = 4$. However, in this research for simplification, 2 level set functions are used to only represent 2 material phases:

$$Vol_1 = \int_D H(\Phi_1) d\Omega \quad , \quad Vol_2 = \int_D H(\Phi_1) H(\Phi_2) d\Omega. \tag{8}$$

Here, Vol_1 is utilized to calculate the total volume and Vol_2 is used to calculate one of the two separate material volumes. The other material volume can be easily achieved by finding the difference between these two.

When combined with the gradient-based optimizer MMA, the derivatives of the objective function and the constrains with respect to the design variable have to be calculated through the sensitivity analysis [43, 44]. By given a pseudo time interval t and considering a two-material structure, the derivative of J in Eq.5 can be expressed as [45]:

$$\left. \frac{dJ}{dt} \right|_{\Phi_k} = \sum_{j=1}^{m} \left(\int_D \beta^k \Psi_j d\Omega \frac{d\mu_{kj}(t)}{dt} \right), \quad k = 1, 2, \tag{9}$$

where β^k takes the form:

$$\beta^k = -\boldsymbol{\varepsilon}(\boldsymbol{u}) : \frac{\partial \boldsymbol{D}(\boldsymbol{x}, \Phi)}{\partial \Phi_k} : \boldsymbol{\varepsilon}(\boldsymbol{u}) \tag{10}$$

By applying the chain rule, the derivative of the objective function with respect to the design variables can be expressed as:

$$\frac{\partial J}{\partial \mu_j^k} = \int_D \beta^k \Psi_j d\Omega, \quad (j = 1, ..., m; \quad k = 1, 2) \tag{11}$$

Similarly, the derivatives for the volume constraints can be achieved in a similar manner:

$$\frac{dVol_1}{d\mu_{1j}} = \int_D \delta(\Phi_1)) \Psi_j d\Omega \quad j = 1, ..., m \tag{12}$$

$$\frac{dVol_1}{d\mu_{2j}} = \int_D \delta(\Phi_1) H(\Phi_2) \Psi_j d\Omega \quad j = 1, ..., m \tag{13}$$

$$\frac{dVol_2}{d\mu_{2j}} = \int_D \delta(\Phi_2) H(\Phi_1) \Psi_j d\Omega \quad j = 1, ..., m \tag{14}$$

To optimize the material properties of the two constructing material along with the topology of the entire structure, the material properties can be treated as design variables [39]. The corresponding derivatives are achieved via the forward finite difference scheme. In a general form, the derivative of function f at point $\boldsymbol{x}$ can be defined as:

$$f'(\boldsymbol{x}) = \lim_{h\to 0} \frac{f(\boldsymbol{x}+h) - f(\boldsymbol{x})}{h}. \tag{15}$$

An energy functional can be minimized along with the objective function to maintain the distance-regularized level set function. The readers can be referred to our previous works [30, 36] regarding the energy functional formulation and derivatives.

4 Formulations for Optimization and Conformal Mapping of Isotropic Metamaterials

With the optimal material properties achieved in the previous stage, in this section, the structural topology optimization of the metamaterial [39] is introduced. To ensure the isotropy of the metamaterial, an extra isotropy constraint is included in the least square optimization statement:

$$\begin{aligned} \text{Min:} \quad & J_{meta} = \frac{1}{2}\sum_{ijkl}^{n}(C^H_{ijkl} - C^*_{ijkl})^2 \\ \text{s.t.:} \quad & \int_D H(\Phi)d\Omega \le Vol_t \\ & a(\boldsymbol{u},\boldsymbol{v},\Phi) = l(\boldsymbol{v},\Phi) \\ & C^*_{1212} = (C^H_{1111} + C^H_{2222})/4 - C^H_{1122}/2 \end{aligned} \quad . \tag{16}$$

Here the Φ is the corresponding level set function for the metamaterial design. The C^H_{ijkl} is the homogenized elasticity tensors with the targets at C^*_{ijkl}. The volume of the metamaterial is constrained by the volume target Vol_t. The structural isotropy [46] is ensured when the condition of $C^*_{1212} = (C^H_{1111} + C^H_{2222})/4 - C^H_{1122}/2$ is satisfied. With the strain energy method, the derivatives can be calculated by using the strain energy under different loading scenarios. The details of this process can be found in [39].

With the optimal overall layout of the multimaterial structure and the detailed layout of the metamaterials, the multimaterial, multiscale structure can be formulated by the local shape-preserving conformal mapping [47]. Some similar works can be found in [48]. The angle-preserving effect of conformal mapping can be illustrated as follows. As can be seen from Figure 2, the pattern on the human face freeform surface in Figure 2(b) still keeps the angles of the checkerboard from Figure 2(a). That is to say the properties can be preserved after the mapping when the boxes are considered as metamaterial unit cells. Below are some basic information about the multiple control point conformal mapping. Let $\omega = f(z) : \mathbb{C} \to \mathbb{C}$ be a complex function on the plane. Denote:

$$\frac{\partial}{\partial \bar{z}} := \frac{1}{2}\left(\frac{\partial}{\partial x} + i\frac{\partial}{\partial y}\right), \tag{17}$$

where i is the unit imaginary root. Then f is said to be *conformal* if

$$\frac{\partial f}{\partial \bar{z}} = 0. \tag{18}$$

Under discrete settings, conformal mappings can be computed by discrete Ricci flow method [49, 50, 51]. Some more discrete Ricci flow algorithms regarding efficiency and adaptivity improvements are reported in [52, 53]. For further conformal mapping algorithms, the readers are refereed to [54] for more information..

The isotropy of the metamaterails will be insensitive to the rotation caused by the mapping and the angle preserving characteristic will ensure the consistency of the designed metamaterial properties. When a highly distorted area has to be mapped, the sharp corners need to be taken care of. By introducing multiple control points, the adaptivity of the mapping to the area distortions can be improved.

Given a triangular mesh $\Sigma = (V, F, E)$, a face element is denoted with corner vertex v_i, v_j and v_k by f_{ijk}, and the angle between rays are denoted as $\overrightarrow{ij}$ and $\overrightarrow{ik}$ by θ_i^{jk}. Then the discrete Gaussian curvature at vertex v_i is defined by

$$K_i = \begin{cases} 2\pi - \sum_{f_{ijk}\in F} \theta_i^{jk} & \text{if } v_i \notin \partial\Sigma, \\ \pi - \sum_{f_{ijk}\in F} \theta_i^{jk} & \text{if } v_i \in \partial\Sigma, \end{cases} \tag{19}$$

where $\partial\Sigma$ is the boundary of mesh Σ. Now the discrete Ricci flow is defined as follows. Given a circle packing metric to Σ, i.e on each vertex v_i a positive real number is defined as γ_i, then the edge length between vertices v_i and v_j is $l_{ij} = \gamma_i + \gamma_j$. With those parameters, all angles can be calculated in Σ. Denote $u_i = \log \gamma_i$, then the discrete Ricci flow is defined as

$$\frac{du_i(t)}{dt} = (\bar{K}_i - K_i), \tag{20}$$

where $\bar{\boldsymbol{k}} = (\bar{K}_1, \bar{K}_2, \ldots, \bar{K}_n)^{\boldsymbol{T}}$ is the user defined target curvature.

In our case, a conformal mapping from a irregular planar region to a polygonal region needs to be found such that the inner angles are either $\pi/2$ or $3\pi/2$. The polygonal region is filled with regular metamaterial structures, and then they are mapped back with the inverse of the computed conformal mapping, which is also a conformal mapping that preserves local shapes. To realize this, on the boundary of input mesh $\partial\Sigma$, multiple control points $W := \{w_1, w_2, \ldots, w_k\} \subseteq \partial\Sigma$ can be selected based on the need.

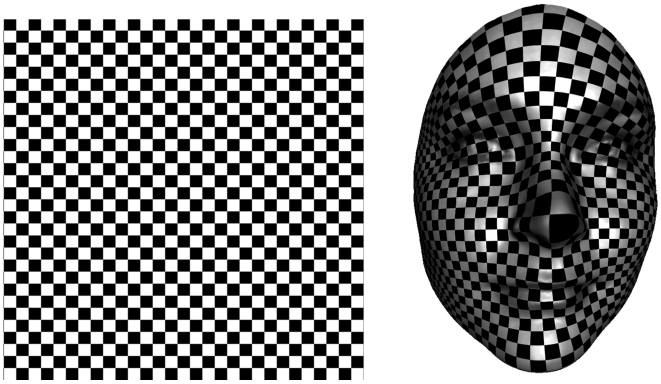

(a) (b)

FIGURE 2. The conventional conformal mapping Ricci flow method. (a) The Checkerboard Pattern. (b) The Freeform Surface.

Then the target curvature on each vertex are defined by:

$$\bar{K}_i = \begin{cases} 0 & \text{if } v_i \notin \partial\Sigma, \\ 0 & \text{if } v_i \in \partial\Sigma \setminus W, \\ -\pi/2 \text{ or } \pi/2 & \text{if } v_i \in W. \end{cases} \tag{21}$$

Here $\bar{K}_i = \pi/2$ is chosen if the target polygonal region has a outward right angle and $\bar{K}_i = -\pi/2$ is chosen if the target polygonal region has a inward right angle at point v_i. Compared to Ricci flow method, as shown in Figure 2, which will map the input region to a freeform surface via four control points, the proposed multi-control-point method provides more flexibility with the benefit of lower area distortion. The detailed information and the mapping work flow can be found in our recent paper [39].

5 Numerical Results

5.1 MBB Beam

In this section, a multimaterial MBB beam structure is designed under the CBF-based concurrent PLSM framework. The macroscale topology optimization boundary condition is illustrated in Figure 3. A $F = 1$ force is applied at the lower center of a 2-by-1 domain with fixed lower corners. The domain is discretized into 100×50 elements. The Young's modulus of the soft material is given the range from 0.05 to 0.1 and the hard one is between 0.15 and 0.2. The initial Young's modulus values of the soft material and the hard material are given 0.075 and 0.175, respectively. The overall material volume is constrained at 60% and the hard material volume is constrained at 30%. The convergence history of the optimization process is shown in Figure 4. The total and the hard material volume for the final design is 59.995% and 29.995%, respectively. The Poisson's ratio for all materials are set to be 0.3. The optimal Young's modulus for the soft metamaterial is 0.1 and the hard one is 0.2, respectively. By using these two values as targets, the second topology optimization is carried out to get the isotropic metamaterial layouts. The Young's modulus for constructing both metamaterials is the same at 1. The volume is 30% and 40% for the soft and hard metamaterial, respectively. A bounding box is introduced to the metamaterials to ensure the connectivity of the adjacent metamaterial unit cells. An isotropy polar plot scheme, as shown in Figure 5, is utilized to illustrate the isotropy of the designed metamaterials, since it is not practical to hit all the targets in the least square objective function in Eq.16. The details of this plot can be found in [39]. By using the conformal mapping, the mapped MBB beam structure is illustrated in Figure 6. By exporting the conformally-mapped structure as a CAD model and send it into FEA package, the actual structural performance can be calculated as 86.29, compared with 72.3939 in Figure 4. For more details about exporting the CAD model and the FEA analysis, the readers are referred to our further journal version of this paper.

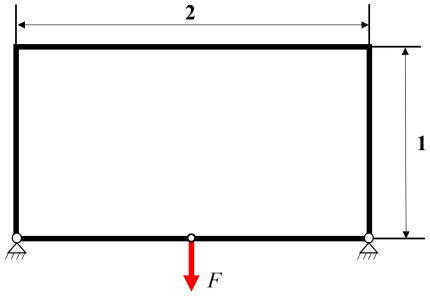

FIGURE 3. The Boundary Condition of the MBB Beam Structure Example

5.2 Michell-type Structure

In this section, the Michell-type structure is designed with the boundary condition shown in Figure 7. With the same optimization setting, the structure topology optimization is carried out with the total volume constraint of 80% and the hard material volume constraint of 40%. The evolution of the design is shown in Figure 8, with the optimal Young's modulus of 0.1 and 0.2 for the soft and hard metamaterial, respectively. The final structure has the total volume of 80% and the hard material volume is 39.992%. The corresponding conformally mapped multiscale structure is shown in Figure 9. The corresponding FEA verification calculates the actual total strain energy as 121.42, compared with 102.5102 shown in Figure 8.

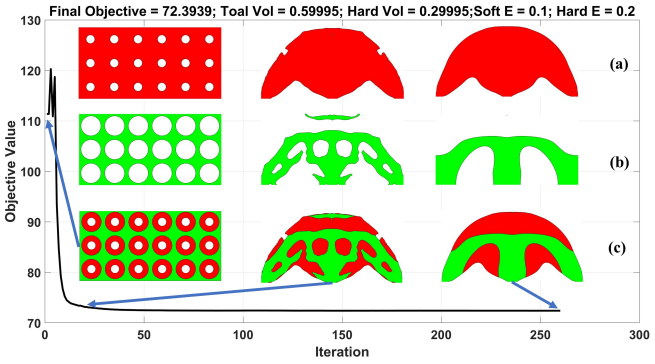

FIGURE 4. The Evolution History of the MBB Beam Structure Example. (a) The Evolution History of the First Zero-Level Set Function. (b) The Evolution History of the Second Zero-Level Set Function. (c) The Evolution History of the Actual Multimaterial Structure. Red: Soft Material. Green: Hard Material.

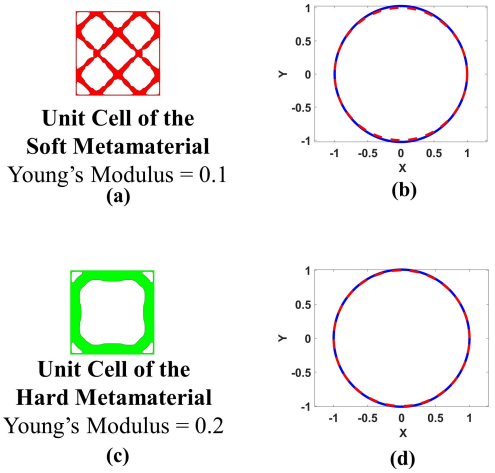

FIGURE 5. Metamaterials and their isotropy plot. (a) The Soft Metamaterial. (b) The Isotropy Polar Plot of the Soft Metamaterial. (c) The Hard Metamaterial. (d) The Isotropy Polar Plot of the Hard Metamaterial. (Red: Reference Standard Circle. Blue: Isotropy Polar Plot of the Current Metamaterial.)

5.3 Short Cantilever Beam

In this section, the short cantilever beam structure is designed within a 1-by-1 design domain discretized into 50×50 elements. The boundary conditions are shown in Figure 10. The material property settings and the topology optimization settings are kept the same as the previous ones. The total volume constraint is 80% and the hard material volume constraint is 40%.

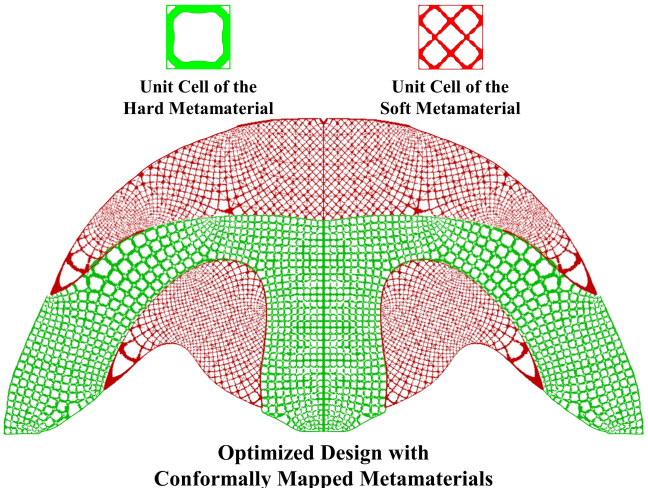

FIGURE 6. The Optimized MBB Beam Structure with Conformally Mapped Hard (Red) and Soft (Green) Metamaterials.

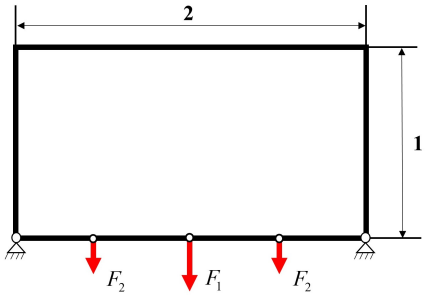

FIGURE 7. The Boundary Condition of the Michell-type Structure Example

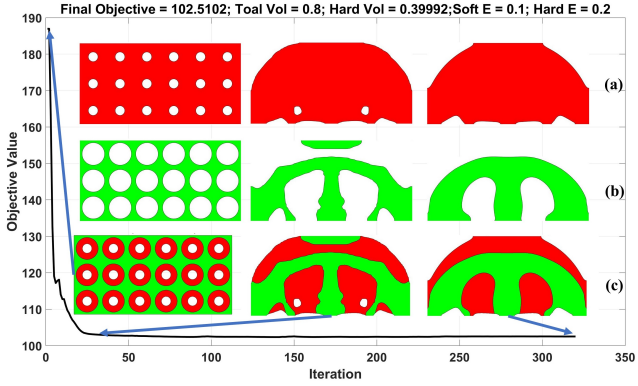

FIGURE 8. The Evolution History of the Michell-Type Beam Structure Example. (a) The Evolution History of the First Zero-Level Set Function. (b) The Evolution History of the Second Zero-Level Set Function. (c) The Evolution History of the Actual Multimaterial Structure. Red: Soft Material. Green: Hard Material.

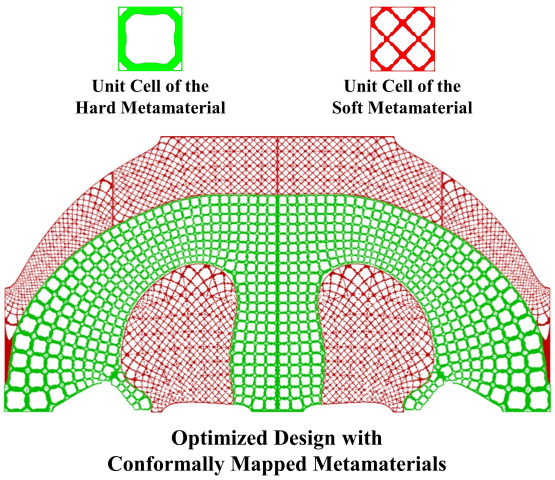

FIGURE 9. The Michell-type Structure with Conformally Mapped Hard (Green) and Soft (Red) Metamaterials.

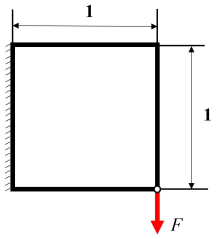

FIGURE 10. The Boundary Condition of the Short Cantilever Beam

The evolution of the design is shown in Figure 11. The final design has the total volume of 79.972% and the hard material volume of 39.989%, together with the optimized Young's modulus of 0.1 and 0.2 for the soft and hard metamaterial, respectively. The corresponding conformally mapped multiscale structure is shown in Figure 12. The corresponding total strain energy for the conformally-mapped structure is calculated as 71.12 in FEA, compared with 67.7091 as shown in Figure 11.

6 Conclusions

In this paper, a concurrent CBF-based PLSM topology optimization framework is proposed to design multimaterial hierarchical structures. With the 'color' level set representation, multiple material phases can be discriminated inside the design domain. By using the CBF kernel function, the explicit design variable bounds can be passed to MMA. The proposed approach can handle multiple constraints in a straightforward manner. With the help of the local shape-preserving conformal mapping with multiple control points, the designed metamaterial properties can be mathematically preserved after the mapping when the isotropic metamaterials are used. The FEA analysis results verify the high fidelity of the proposed mapping scheme. Therefore, the designing-mapping-manufacturing process is concluded.

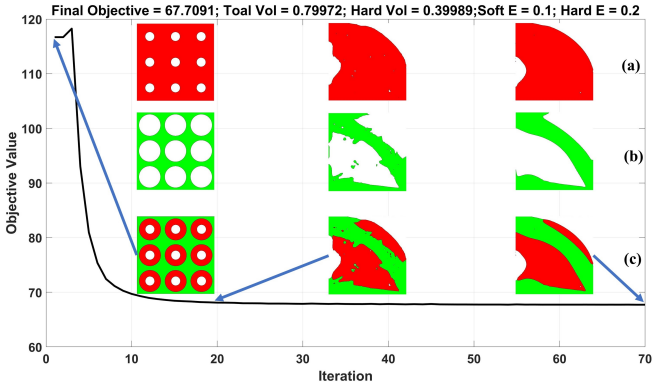

FIGURE 11. The Evolution History of the Short Cantilever Beam Structure Example. (a) The Evolution History of the First Zero-Level Set Function. (b) The Evolution History of the Second Zero-Level Set Function. (c) The Evolution History of the Actual Multimaterial Structure. Red: Soft Material. Green: Hard Material.

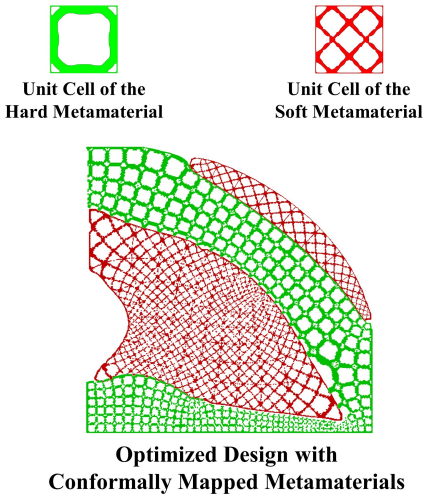

FIGURE 12. The Short Cantilever Beam Structure with Conformally Mapped Hard (Green) and Soft (Red) Metamaterials

ACKNOWLEDGMENT

The authors acknowledge the support from the National Science Foundation of the United States (Grants No. CMMI1462270 and CMMI1762287), Ford University Research Program (URP), and the start-up fund from the State University of New York at Stony Brook. The authors would also like to thank Mr. Yang Guo from the Department of Computer Science at Stony Brook University for his help with the implementation of the conformal mapping method in this paper.

REFERENCES

[1] Fullwood, D. T., Niezgoda, S. R., Adams, B. L., and Kalidindi, S. R., 2010. "Microstructure sensitive design for performance optimization". *Progress in Materials Science,* ***55***(6), pp. 477–562.

[2] Deng, J., Yan, J., and Cheng, G., 2013. "Multi-objective concurrent topology optimization of thermoelastic structures composed of homogeneous porous material". *Structural and Multidisciplinary Optimization,* ***47***(4), pp. 583–597.

[3] Vlasea, M., Shanjani, Y., Bothe, A., Kandel, R., and Toyserkani, E., 2013. "A combined additive manufacturing and micro-syringe deposition technique for realization of bioceramic structures with micro-scale channels". *The International Journal of Advanced Manufacturing Technology,* ***68***(9-12), pp. 2261–2269.

[4] Sigmund, O., 2001. "Design of multiphysics actuators using topology optimization–part ii: Two-material structures". *Computer methods in applied mechanics and engineering,* ***190***(49-50), pp. 6605–6627.

[5] Sigmund, O., and Torquato, S., 1996. "Composites with extremal thermal expansion coefficients". *Applied Physics Letters,* ***69***(21), pp. 3203–3205.

[6] Sigmund, O., and Maute, K., 2013. "Topology optimization approaches". *Structural and Multidisciplinary Optimization,* ***48***(6), pp. 1031–1055.

[7] Allaire, G., Jouve, F., and Toader, A.-M., 2002. "A level-set method for shape optimization". *Comptes Rendus Mathematique,* ***334***(12), pp. 1125–1130.

[8] Wang, M. Y., Wang, X., and Guo, D., 2003. "A level set method for structural topology optimization". *Computer methods in applied mechanics and engineering,* ***192***(1-2), pp. 227–246.

[9] Sethian, J. A., and Wiegmann, A., 2000. "Structural boundary design via level set and immersed interface methods". *Journal of computational physics,* ***163***(2), pp. 489–528.

[10] van Dijk, N. P., Maute, K., Langelaar, M., and Van Keulen, F., 2013. "Level-set methods for structural topology optimization: a review". *Structural and Multidisciplinary Optimization,* ***48***(3), pp. 437–472.

[11] Sethian, J. A., 1996. "Theory, algorithms, and applications of level set methods for propagating interfaces". *Acta numerica,* ***5***, pp. 309–395.

[12] Wang, M. Y., and Wang, X., 2004. ""color" level sets: a multi-phase method for structural topology optimization with multiple materials". *Computer Methods in Applied Mechanics and Engineering,* ***193***(6-8), pp. 469–496.

[13] Wei, P., and Wang, M. Y., 2009. "Piecewise constant level set method for structural topology optimization". *International Journal for Numerical Methods in Engineering,* ***78***(4), pp. 379–402.

[14] Merriman, B., Bence, J. K., and Osher, S. J., 1994. "Motion of multiple junctions: A level set approach". *Journal of Computational Physics,* ***112***(2), pp. 334–363.

[15] Gibson, L. J., and Ashby, M. F., 1999. *Cellular solids: structure and properties*. Cambridge university press.

[16] Christensen, R. M., 2000. "Mechanics of cellular and other low-density materials". *International Journal of Solids and Structures,* ***37***(1-2), pp. 93–104.

[17] Valdevit, L., Jacobsen, A. J., Greer, J. R., and Carter, W. B., 2011. "Protocols for the optimal design of multifunctional cellular structures: From hypersonics to microarchitected materials". *Journal of the American Ceramic Society,* ***94***(s1).

[18] Han, S. C., Lee, J. W., and Kang, K., 2015. "A new type of low density material: shellular". *Advanced Materials,* ***27***(37), pp. 5506–5511.

[19] Zhou, S., Li, W., Chen, Y., Sun, G., and Li, Q., 2011. "Topology optimization for negative permeability metamaterials using level-set algorithm". *Acta Materialia,* ***59***(7), pp. 2624–2636.

[20] Wang, Y., Luo, Z., Zhang, N., and Kang, Z., 2014. "Topological shape optimization of microstructural metamaterials using a level set method". *Computational Materials Science,* ***87***, pp. 178–186.

[21] Vogiatzis, P., Chen, S., Wang, X., Li, T., and Wang, L., 2017. "Topology optimization of multi-material negative poisson's ratio metamaterials using a reconciled level set method". *Computer-Aided Design,* ***83***, pp. 15–32.

[22] Zhou, S., Li, W., Sun, G., and Li, Q., 2010. "A level-set procedure for the design of electromagnetic metamaterials". *Optics express,* ***18***(7), pp. 6693–6702.

[23] Wang, Y., Gao, J., Luo, Z., Brown, T., and Zhang, N., 2017. "Level-set topology optimization for multimaterial and multifunctional mechanical metamaterials". *Engineering Optimization,* ***49***(1), pp. 22–42.

[24] Sivapuram, R., Dunning, P. D., and Kim, H. A., 2016. "Simultaneous material and structural optimization by multiscale topology optimization". *Structural and multidisciplinary optimization,* ***54***(5), pp. 1267–1281.

[25] Wang, Y., Chen, F., and Wang, M. Y., 2017. "Concurrent design with connectable graded microstructures". *Computer Methods in Applied Mechanics and Engineering,* ***317***, pp. 84–101.

[26] Li, H., Luo, Z., Gao, L., and Qin, Q., 2018. "Topology optimization for concurrent design of structures with multipatch microstructures by level sets". *Computer Methods in Applied Mechanics and Engineering,* ***331***, pp. 536–561.

[27] Allaire, G., Jouve, F., and Toader, A.-M., 2004. "Structural optimization using sensitivity analysis and a level-set method". *Journal of computational physics,* ***194***(1), pp. 363–393.

[28] Osher, S. J., and Santosa, F., 2001. "Level set methods for optimization problems involving geometry and constraints:

I. frequencies of a two-density inhomogeneous drum". *Journal of Computational Physics,* ***171***(1), pp. 272–288.

[29] Osher, S., and Sethian, J. A., 1988. "Fronts propagating with curvature-dependent speed: algorithms based on hamilton-jacobi formulations". *Journal of computational physics,* ***79***(1), pp. 12–49.

[30] Jiang, L., and Chen, S., 2017. "Parametric structural shape & topology optimization with a variational distance-regularized level set method". *Computer Methods in Applied Mechanics and Engineering,* ***321***, pp. 316–336.

[31] Luo, Z., Tong, L., Wang, M. Y., and Wang, S., 2007. "Shape and topology optimization of compliant mechanisms using a parameterization level set method". *Journal of Computational Physics,* ***227***(1), pp. 680–705.

[32] Wang, S., and Wang, M. Y., 2006. "Radial basis functions and level set method for structural topology optimization". *International journal for numerical methods in engineering,* ***65***(12), pp. 2060–2090.

[33] Svanberg, K., 2007. "Mma and gcmma-two methods for nonlinear optimization". *vol,* ***1***, pp. 1–15.

[34] Jiang, L., Ye, H., Zhou, C., Chen, S., and Xu, W., 2017. "Parametric topology optimization toward rational design and efficient prefabrication for additive manufacturing". In ASME 2017 12th International Manufacturing Science and Engineering Conference collocated with the JSME/ASME 2017 6th International Conference on Materials and Processing, American Society of Mechanical Engineers, pp. V004T05A006–V004T05A006.

[35] Luo, Z., Wang, M. Y., Wang, S., and Wei, P., 2008. "A level set-based parameterization method for structural shape and topology optimization". *International Journal for Numerical Methods in Engineering,* ***76***(1), pp. 1–26.

[36] Jiang, L., Chen, S., and Jiao, X., 2018. "Parametric shape and topology optimization: A new level set approach based on cardinal basis functions". *International Journal for Numerical Methods in Engineering,* ***114***(1), pp. 66–87.

[37] Li, C., Xu, C., Gui, C., and Fox, M. D., 2010. "Distance regularized level set evolution and its application to image segmentation". *IEEE transactions on image processing,* ***19***(12), pp. 3243–3254.

[38] Jiang, L., Chen, S., and Wei, P., 2018. "Concurrent optimization of structure topology and infill properties with a cardinal-function-based parametric level set method". In ASME 2018 International Design Engineering Technical Conferences and Computers and Information in Engineering Conference, American Society of Mechanical Engineers, pp. V02BT03A006–V02BT03A006.

[39] Jiang, L., Guo, Y., Chen, S., Wei, P., Lei, N., and Gu, X. D., 2019. "Concurrent optimization of structural topology and infill properties with a cbf-based level set method". *Frontiers of Mechanical Engineering*, pp. 1–19.

[40] Challis, V., Roberts, A., and Wilkins, A., 2008. "Design of three dimensional isotropic microstructures for maximized stiffness and conductivity". *International Journal of Solids and Structures,* ***45***(14-15), pp. 4130–4146.

[41] Radman, A., Huang, X., and Xie, Y., 2013. "Topological optimization for the design of microstructures of isotropic cellular materials". *Engineering optimization,* ***45***(11), pp. 1331–1348.

[42] Guth, D., Luersen, M., and Muñoz-Rojas, P., 2015. "Optimization of three-dimensional truss-like periodic materials considering isotropy constraints". *Structural and Multidisciplinary Optimization,* ***52***(5), pp. 889–901.

[43] Van Keulen, F., Haftka, R., and Kim, N., 2005. "Review of options for structural design sensitivity analysis. part 1: Linear systems". *Computer methods in applied mechanics and engineering,* ***194***(30-33), pp. 3213–3243.

[44] Choi, K. K., and Kim, N.-H., 2006. *Structural sensitivity analysis and optimization 1: linear systems*. Springer Science & Business Media.

[45] Wang, Y., Luo, Z., Kang, Z., and Zhang, N., 2015. "A multi-material level set-based topology and shape optimization method". *Computer Methods in Applied Mechanics and Engineering,* ***283***, pp. 1570–1586.

[46] Neves, M., Rodrigues, H., and Guedes, J. M., 2000. "Optimal design of periodic linear elastic microstructures". *Computers & Structures,* ***76***(1-3), pp. 421–429.

[47] Ahlfors, L. V., 2010. *Conformal invariants: topics in geometric function theory*, Vol. 371. American Mathematical Soc.

[48] Wang, H., Chen, Y., and Rosen, D. W., 2005. "A hybrid geometric modeling method for large scale conformal cellular structures". In ASME Computers and Information in Engineering Conference, Long Beach, CA, Sept, pp. 24–28.

[49] Jin, M., Kim, J., Luo, F., and Gu, X., 2008. "Discrete surface ricci flow". *IEEE Transactions on Visualization and Computer Graphics,* ***14***(5), pp. 1030–1043.

[50] Chow, B., Luo, F., et al., 2003. "Combinatorial ricci flows on surfaces". *Journal of Differential Geometry,* ***63***(1), pp. 97–129.

[51] Zeng, W., and Gu, X. D., 2013. *Ricci flow for shape analysis and surface registration: theories, algorithms and applications*. Springer Science & Business Media.

[52] Gu, X., He, Y., Jin, M., Luo, F., Qin, H., and Yau, S.-T., 2008. "Manifold splines with a single extraordinary point". *Computer-Aided Design,* ***40***(6), pp. 676–690.

[53] Jin, M., Luo, F., and Gu, X., 2006. "Computing surface hyperbolic structure and real projective structure". In Proceedings of the 2006 ACM symposium on Solid and physical modeling, ACM, pp. 105–116.

[54] Gu, X. D., Zeng, W., Luo, F., and Yau, S.-T., 2012. "Numerical computation of surface conformal mappings". *Computational Methods and Function Theory,* ***11***(2), pp. 747–787.